Eurographics Workshop on Visual Computing for Biology and Medicine (2018)
A. Puig Puig, T. Schultz, and A. Vilanova (Editors)

Estimation of Muscle Activity in One-Leg Stance from 3D Surface Deformation †

Johannes Metzler‡, Thomas Neumann‡, Stefanie Gassel, Jens Friedrich, Markus Wacker

University of Applied Science (HTW) Dresden, Germany

Abstract

Muscular activity during human motion is usually quantified by measuring the electrical potential during muscle activation using electromyography (EMG). However, apart from producing electrical activity, muscular contraction of many skeletal muscles also induces subtle deformation of the skin surface. In this paper, we present a method to estimate muscular activation from such 3D skin deformation. To this end, we introduce a capture system that reconstructs the 3D motion of the skin from multi-view video data and simultaneously measures true muscle activity with EMG sensors. Our data reveals strong correlations between the skin deformation and muscular activity during one-leg stances. We propose a pose normalization procedure and a novel model based on Supervised Principal Component Regression that automatically segments individual muscles and estimates their activation from 3D surface deformation. Our evaluation shows that the model generalizes to varying body shapes and that the estimated activation closely fits the measured EMG data.

CCS Concepts

•***Applied computing*** → ***Life and medical sciences;***

1. Introduction

Estimating muscular activity is one of the most important tasks to understand and assess human motion, with applications in ergonomics, kinesiology, biomechanics, and even for clinical diagnosis of neuromuscular diseases. The gold standard method to quantify muscle activations is electromyography (EMG) that measures electrical activity emitted by muscle cells when neurologically activated [LRI74], essentially by sticking an electrode onto the skin surface or into the muscle fiber. However, this measurements are expensive, can only be applied pointwise, and the installation requires trained specialists. This restricts practicability in everyday clinical and research life. However, activation of some human muscles produces subtle deformation that become visible on the skin surface. In this paper, we show that from measurements of such deformations on the 3D skin surface it is possible to estimate underlying muscular activity.

In particular, we focus on muscle activity estimation during balance tests due to their wide use. For example, the one-leg stance is used to measure the postural stability of individuals [FMV00], with applications in rehabilitation, training and geriatrics [ZHV*10, HRW*00], e.g. as indicator for the risk of falling. Maintaining body balance requires constant coordinated activation of a multitude of muscles mostly in the lower leg. Skin deformation during one-leg stances is extremely subtle, in the range of at most a few millimeters. State-of-the-art markerless performance capture systems are able to reconstruct full body human geometry in motion at high visual fidelity [TdAS*10], but are not yet able to reconstruct sub-millimeter precise skin surface deformation. We thus opt for the marker based system of Neumann *et al.* [NVH*13], that we extend to achieve even higher detail. In addition, we simultaneously record muscle activity using synchronized EMG sensors, in order to relate these signals to the visible skin deformation. In this study, we need such a high-end recording system, because it is not yet clear which level of detail is required for muscle activity estimation.

In the analysis process, we isolate the surface deformation by subtracting rigid motion of the limbs using an effective pose normalization step. The resulting data reveals strong correlations between visible muscle deformation and electrical activity especially in the muscles *Peroneus longus* (Figure 3a) and *Tibialis anterior* (Figure 3b). We use the data to train a model that automatically estimates muscle activity from the 3D surface recordings. To this end, we extend Supervised Principal Component Regression [BHPT06] with a Graph-Cut based mesh segmentation method. Finally, we demonstrate that the model can estimate muscular activity and also generalizes to different body shapes.

† This work was supported in part by ESF (grant number 100231931, TISRA).

‡ These two authors contributed equally

DOI: 10.2312/vcbm.20181241

In summary, our contributions are:

- a system to simultaneously measure muscle activity (using EMG) and detailed dynamic 3D geometry of muscles at sub-millimeter precision (using an improved version of the video-based system of Neumann *et al.* [NVH*13])
- a model based on Supervised Principal Component Regression with a Graph-Cut based mesh segmentation to estimate muscular activity.

This research has the longer-term goal of supplementing the EMG technology with a camera-based tracking method. A camera-based system would significantly reduce the cost of such a measurement and make it applicable for more facilities. In addition, temporally and spatially synchronized records of skin surface data may provide a new modality for gait analysis applications. While the EMG procedure can measure muscle activity only very locally, our measurement method is surface-based and may be able to reveal yet unkown spatio-temporal muscle behavior patterns. For example, it could be possible to analyze where certain muscle deformation take place on the skin or exactly how the muscle volume and shape change during exercise, which is not yet possible with EMG.

2. Related Work

Estimation of muscular activity is usually studied in the fields of biomechanics. The gold standard is EMG recording, which is an electrodiagnostic medicine technique for evaluating and recording the electrical activity produced by skeletal muscles. There are two kinds of EMG: surface EMG [De 97] and invasively intramuscular EMG [PS02]. Surface EMG assesses muscle function by recording muscle activity with electrodes on the skin. These can only provide a limited assessment of the muscle activity. In contrast, intramuscular EMG needles can be positioned precisely to record individual muscle fibers, at the cost of being highly invasive. Muscular activity may also be inferred indirectly with ultrasound recordings [HPHG03], where muscle volume or elongation during activation can be (manually) segmented. These measurements showed that muscle activity and volume change are linearly correlated only for small forces up to 30%. At higher levels of contraction, the muscle volume changes relatively little. Since the muscle activity in the one-leg stance is rather small, it can be considered as linear with the volume change. Another study investigates the physiological oddity in facial muscles of subjects with Autism Spectrum Disorder in comparison to that of a control [SBHI15] group. However, this study is limited to static facial expressions. Only recent studies showed that muscle activity may be estimated from images [ABF15] or from shape changes captured by depth sensors [SYA*16]. However, these approaches are limited in their evaluation since the model was trained and tested on the same person. Their models are relatively black-box machine learning models, while ours is a simple supervised PCA regression model that is easily interpretable. We show, that our model also generalizes across multiple subjects and allows fine-grained visualization of the specific skin deformation that correlate with actual muscular activity as measured by EMG.

Simulation-driven muscle simulations in computer graphics aim at generating the skin surface of a virtual character or creature and thus rely on simplified volumetric models of muscle tissue [Lee11]. In contrast, the biomechanics community relies on abstract models containing bones and actuators (muscles/tendons), with a focus on accurate estimation of muscular forces for example with OpenSIM [DAA*07]. OpenSIM's inverse dynamics solves for the muscle forces that are required for the given motion (e.g. captured with a Motion Capture system). OpenSIM models have to be carefully evaluated and calibrated from EMG recordings and work reliably for fast, long-range motions. Additionally, the analysis of the one-leg stance requires ground reaction forces measured by a force plate.

Data-driven muscle simulations generates a muscle deformation model by capturing skin deformation from (dynamic) scans of real people. When animating human characters, data-driven models are often used because they provide a realistic image with little effort [ASK*05, LMR*15]. Neumann *et al.* [NVH*13] were the first to model muscle deformation as a function of external force with a data-driven approach. Gassel *et al.* [GNW17] extend upon this work and link the data-driven model with muscle forces computed from the biomechanical simulation model OpenSIM [DAA*07]. This allows generating plausible deformation of individual muscles given muscle forces. In this work we invert this idea and estimate the muscle activity from the visible muscle deformation. But as common with data-driven models, we require an accurate method for measuring the 3D muscle deformation.

Multi-view performance capture originally aims at reconstructing dynamic geometry of human subjects, possibly including clothing and props [TdAS*10]. State-of-the-art approaches handle very general scenes [CCS*15] and can even run in real-time [DTF*15, IZN*16]. However, these approaches are not yet able to precisely capture muscle deformation, since the subtle muscle deformation cannot be tracked/matched on mostly textureless skin unless the camera resolution is high enough that individual skin pores become visible [BB14]. Several works thus resorted to using markers for capturing the skin surface. Park *et al.* [PH08] use up to 350 conventional motion-capture markers to reconstruct human skin deformation. Bogo *et al.* [BRPMB17] use an expensive 3D scanning setup involving multiple camera-projector rigs to obtain 3D geometry and recover very detailed skin deformation by tracking bodypaint stamps applied to the skin of the subjects. Neumann *et al.* [NVH*13] use a simpler multi-camera setup, paint random dots onto the skin and use them both for 3D reconstruction and tracking. Here, we adopt their approach and show that it can indeed recover muscle twitches up to millimeter accuracy using only 16 HD cameras, with only 12 used for the reconstruction. The other 4 cameras were used for overview purposes. The application of dots on the skin directly is maybe laborious, but is intentionally used here to obtain ground-truth reference data. Later iterations of our approach can instead use pattern-printed tights [WCF07, SSK*05, Neu16] as a close proxy to the skin surface.

Pose normalization is necessary to subtract the rigid motion of the bones from the actual muscle or soft tissue deformation. Some data-

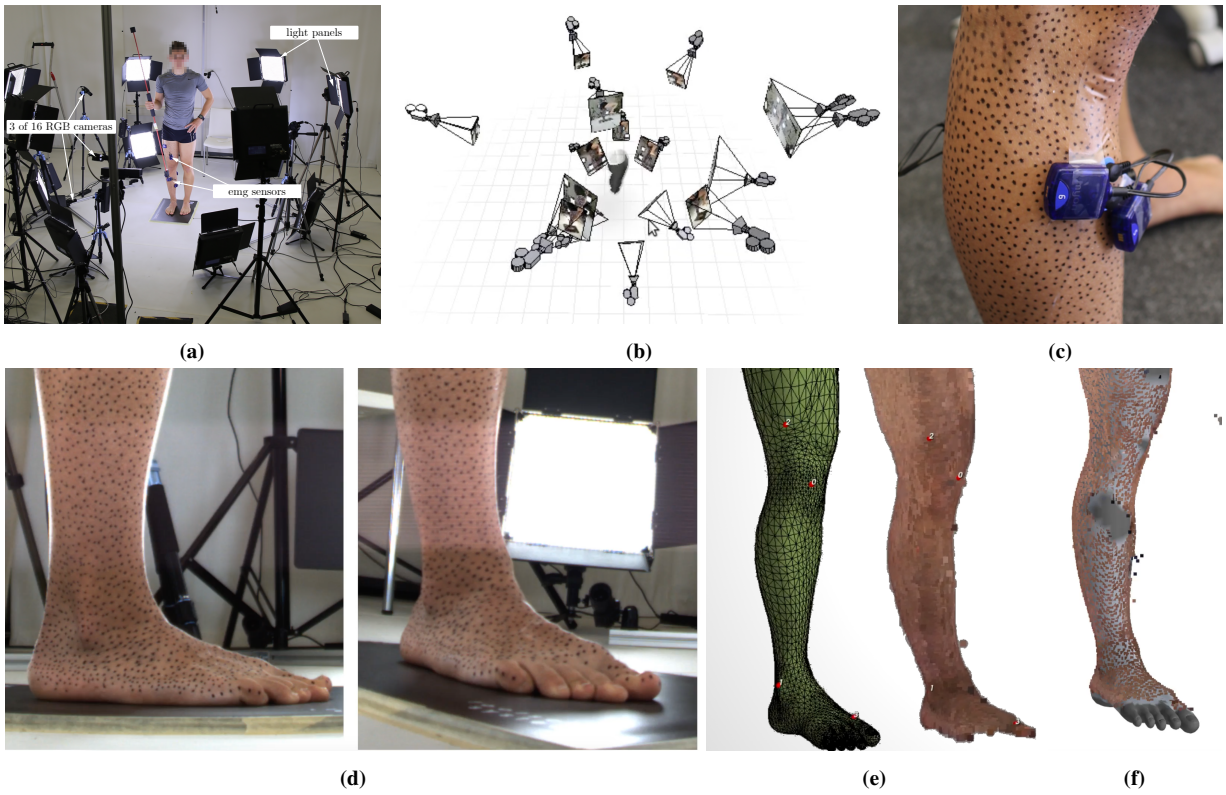

Figure 1: Capturing muscle deformation: (a) Subjects are recorded by a multi-sensor setup consisting of 16 synchronized video cameras. (b) Camera positions after calibration. (c) Wireless EMG sensors simultaneously record electrical activity in the muscles. (d) Stereo pair of cameras showing the random dot pattern on the skin. (e) Template mesh and reconstructed 3D point cloud. (f) Template mesh closely fits point cloud after non-rigid ICP.

driven shape modeling approaches [ASK*05, NVH*13, LMR*15] internally already do this by first applying rigid (body part) rotations and then modeling the residual deformation due to soft tissue and muscle deformation. In other words, they model deformation in pose space [LCF00]. Although not explicitely designed for pose normalization, unsupervised decomposition methods [KSO10, NVW*13] may also be used for extracting pose-specific deformation. Nevertheless, the explicit task of pose normalization of a given captured 3D surface was first formulated by Beeler and Bradley [BB14] for face stabilization. Their approach relies on anatomic constraints specific to human faces and cannot be readily extended to the lower body. To this end, anatomic skin deformation models have been developed for other parts, for example to precisely capture bone motion of the shoulder-arm area from noisy depth sensor measurements [ZHK15]. However, since anatomical based models require significant amount of engineering and since the motion of the leg in our data is not very high, we instead adapt a simple but effective skinning decomposition method [KSO10] to perform a pose normalization, cf. Section 3.2.

3. Data Acquisition

As a basis for further analysis, we developed a new multi-modal capture system to record simultaneously detailed time-varying 3D geometry of human skin and muscular activity. Here, we briefly describe our setup and give an overview of the captured dataset.

3.1. 3D Reconstruction and Registration of Skin Surfaces

To capture skin deformation at high detail, we use a vision-based reconstruction approach that measures dense dynamic 3D geometry with a multi-camera system (cf. Figure 1a). 16 HD cameras (*Grasshopper GRAS-20S4C*) from PointGrey (1600×1200 pixels resolution @ 30 Hz) are arranged in a convergent setup around the lower body (Figure 1b). To facilitate space-time reconstruction, we apply a pattern of dense dots to the skin. (Figure 1d). These dots are reconstructed in 3D using the multi-graph matching method of [NVH*13] with improvements as presented in [Neu16, Section 2.3]. The algorithm delivers a 3D point cloud for each recorded frame. These 3D points are then tracked by matching them across the whole sequence with the affine-invariant modification of Shape Context developed in [NVH*13].

We then bring a template mesh of the lower body (Figure 1e), into correspondence with all the captured 3D point clouds. In particular, we perform non-rigid iterative-closest-point (ICP) with As-rigid-as-possible surface regularization [SA07] using the global formulation of [ZNI*14]. In contrast to [NVH*13], this provides a tighter fit of the mesh in areas where a dense pattern of dots was

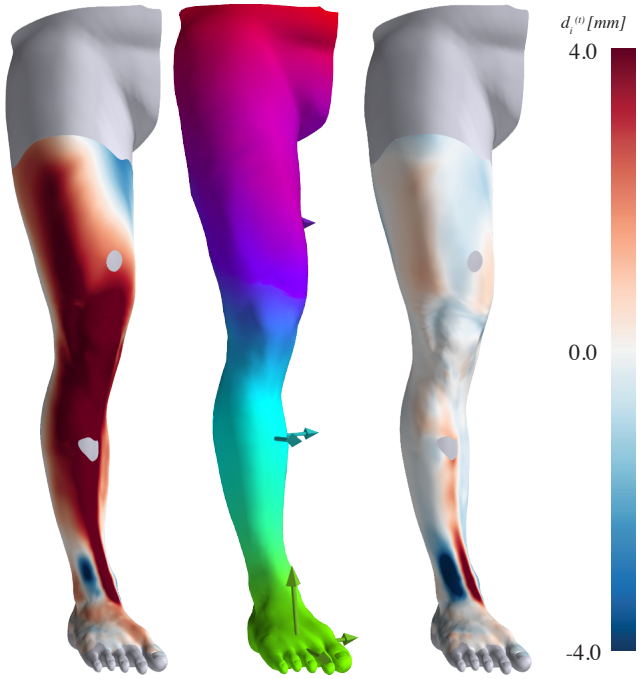

Figure 2: Pose normalization. (a) Displacements from rest shape without pose normalization show mostly rigid motion of the lower leg. (b) Estimated blending weights for body parts to be used for pose normalization (green = foot, cyan = lower leg, violet = upper let, red = hip). (c) After applying these blending weights for pose normalization, muscle and tendon deformation become visible.

visible while properly interpolating in areas where the EMG sensor occluded the dots. As a result, we obtain the deformed template mesh closely fitting to the reconstructed dots (Figure 1f).

3.2. Pose normalization

When directly measuring displacements of the reconstructed 3D mesh from a rest shape, most will be due to rigid motion of the limbs due to the sway of the body around its center of pressure, as visible in Figure 2a. In a last step, we remove pose-related motion of the foot, the lower and the upper leg: we first estimate a segmentation into body parts from a squat motion of the same leg using the method of Kavan et al. [KSO10], cf. Figure 2b. Then, based on this segmentation, a rigid transformation can be estimated for each of the body parts and for each time step. Using linear blend skinning we can apply the inverse transformation at each step for each body part to obtain a mesh sequence with the articulated motion almost entirely removed (cf. Figure 2c). Since every recorded subject stood in a slightly different place, in the last step the subject is aligned by procrustes to the reference subject.

3.3. EMG Recording

We simultaneously measure electrical activity in seven different muscles using the wireless surface EMG sensor Myon 320 by Pro-

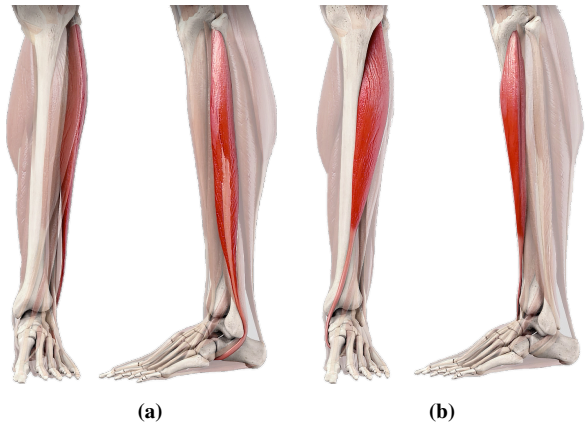

Figure 3: Anatomy of the muscles (a) Peroneus Longus and (b) Tibialis Anterior, pictures provided by *DocCheck* (http://flexikon.doccheck.com)

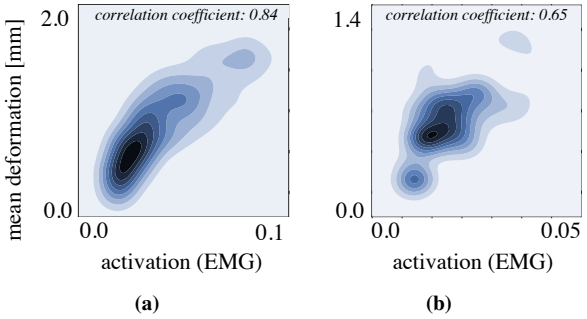

Figure 4: Correlation plot between mean mesh deformation and EMG signal. (a) Tibialis Anterior (b) Peroneus Longus

Physics (https://www.myon.ch). These sensors are attached to the skin of the person and thus give only a rough estimate of the overall activity of muscles that are relatively close to the surface (cf. Section 2, in contrast to intramuscular EMG). EMG sensors were synchronized to the multi-camera system using hardware triggers to start recording: The EMG sensors act as master triggers since they offer the highest refresh rate in this setup. Trigger signals from the EMG are intercepted by an Arduino and passed via USB to the multi-camera setup, which is internally synchronized using the PointGrey MultiCamera API. EMG sensors are attached to the following muscles: Rectus femoris, Vastus medialis, Biceps femoris, Tibialis anterior, Peroneus longus, Soleus and Gastrocnemius. Of these muscles, only *Tibialis anterior* and *Peroneus longus* are typically active during the one-leg stance. EMG data were normalized using a maximum voluntary contraction (MVC) trial (this procedure corrects for typical subject- and muscle-specific variances by expressing EMG measurements relative to the maximal value seen during strong voluntary contraction that we recorded separately). Signals are denoised using a high and low pass butterworth filter followed by notch filtering and root mean square smoothing.

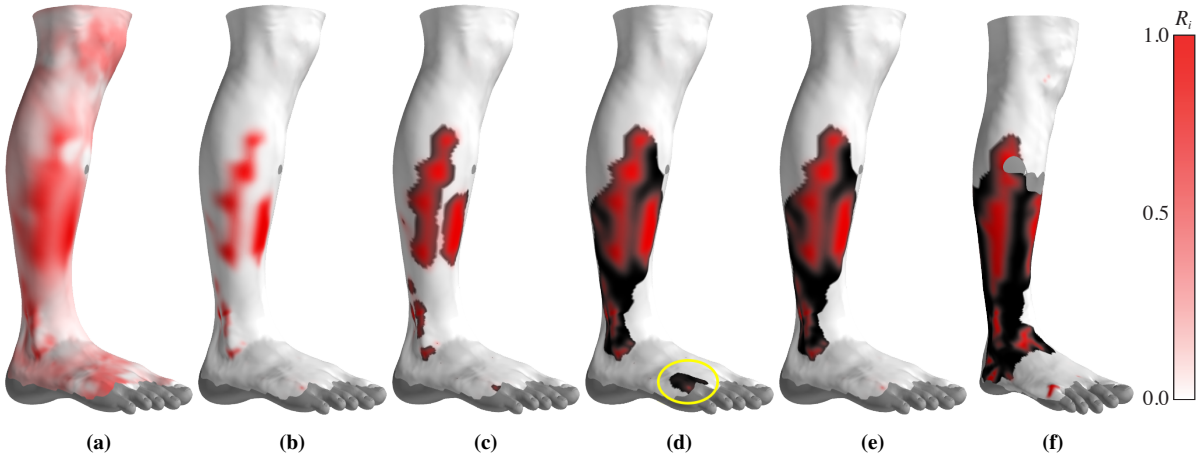

Figure 5: Development of surface mask with graphcut to muscle *Peroneus longus* on *subject 1*. (a) Correlations of the vertices, color-coded in red. (b) Clipped correlations. (c) Simple tresholding. The black mask lies exact under the red correlations. (d) Execution of the graphcut with optimized parameters. The correlations are shown in red above the black mask. (e) Subgraph with largest connected area. This removes the area, that is circled in d. (f) Muscle masking with same parameters on *subject 2*. Mask looks similar.

Subject	Age [years]	Weight [kg]	Sex	Height [cm]
#1	21	81	m	181
#2	56	67	w	173
#3	32	65	m	180
#4	35	70	m	184

Table 1: Overview of the captured subjects.

3.4. Dataset

We recruited 4 subjects, 1 female and 3 male, to be captured, with age varying from 21 to 56 years, cf. Table 1. Each subject performs the same predefined motions. Here, we specifically concentrate the analysis on one-leg stances. For each subject, three repetitions of 16 second long one-leg stances were recorded.

3.5. Explorative Data Analysis

With the simultaneous multi-sensor data at hand, we can now investigate if there is a correlation between electrical activity of the muscles and 3D skin deformation. To this end, the 3D displacement after pose normalization is averaged inside a manually chosen area per muscle. This gives a rough estimate of the overall deformation for each muscle in each recorded video frame. This average deformation already correlates well with the actual EMG signal, as visible from the correlation plots in Figure 4. This important insight motivates the construction of a new model that estimates muscle activity as explained in the following.

4. Model

The correlation analysis (Figure 4) clearly shows correlations between 3D skin deformation and muscular activity measured via EMG. This leds us to build a model that maps the 3D skin deformation to the EMG sensor. To this end, we propose an extension to Supervised PCA [BHPT06]: we first automatically find a local muscle area and then perform Principal Component Regression to linearly predict the EMG signal from the deformation in that area. Once this model has been trained on a subset of subjects from our dataset, it can be applied to predict the muscular activity of new, previously unseen subjects from the skin deformation.

4.1. Preliminaries

Formally, we are given the pose-normalized 3D locations of all $N \in \mathbb{N}$ vertices $\mathbf{v}_i^{(f)} \in \mathbb{R}^3, i \in \{1,\dots,N\}$ for each of the $f \in \{1,\dots,F\}$ recorded mesh surfaces (e.g. successive frames of a one-leg stance motion). During training, we are also given the corresponding EMG signal $\mathbf{y} \in \mathbb{R}^F$ at that each frame. We first need to determine a "rest shape" frame f_0 where the muscle activity is as low as possible (e. g. $f_0 = \arg\min_j \mathbf{y}_j$) to obtain the vertex displacements, $\mathbf{d}_i^{(f)} = \mathbf{v}_i^{(f)} - \mathbf{v}_i^{(f_0)}$ (from hereon, we shall use the word deformation for these vertex displacements). Then we collect all displacements into a displacement matrix $\mathbf{X} \in \mathbb{R}^{F \times 3N}$, by stacking the displacement vectors corresponding to one frame into a single row:

$$\mathbf{X} = \begin{bmatrix} (\mathbf{d}_1^{(1)})^\top & (\mathbf{d}_2^{(1)})^\top & \cdots & (\mathbf{d}_N^{(1)})^\top \\ (\mathbf{d}_1^{(2)})^\top & (\mathbf{d}_2^{(2)})^\top & \dots & (\mathbf{d}_N^{(2)})^\top \\ \vdots & \vdots & \ddots & \vdots \\ (\mathbf{d}_1^{(F)})^\top & (\mathbf{d}_2^{(F)})^\top & \dots & (\mathbf{d}_N^{(F)})^\top \end{bmatrix} \quad (1)$$

In principle, we could directly learn a mapping of the deformation of one frame $\mathbf{X}_{f,\star}$ (f'th row in matrix $\mathbf{X}$) to the EMG readings $\mathbf{y}_f$, but this is prone to overfitting, cf. Figure 9. Principal Component Analysis (PCA) could be used to prevent this, but running PCA directly on $\mathbf{X}$ might still pick up on deformation not related to the specific muscle measured by the EMG sensor. Thus, we provide

only a subset of vertices from $\mathbf{X}$ to PCA that correlate well with the EMG signal $\mathbf{y}$. This general idea of removing irrelevant features before running PCA is known as supervised principal component analysis [BHPT06] (SPCA), where features are selected based on their correlation with the target variable $\mathbf{y}$. However, simply selecting individual vertices performs poorly since the selected area contains many outliers and overfits on the specific area of the subject in the training set, cf. Figure 5c. Therefore, we propose to find a mask that both fits the correlations well and being sufficiently localized and smooth at the same time.

4.2. Masking muscles

We formulate finding a binary muscle mask $\mathbf{m} \in \{0,1\}$ (defined over the vertices) using Graph Cuts optimization [EFS56, GF08]. The graph is defined by the mesh topology. We define unary potentials (for the data term in Graph Cuts optimization) from the coefficient of multiple correlation $R_i \in [0,1]$ [CCWA13] between the vertex i and the EMG signal $\mathbf{y}$, which basically estimates how well a linear model would predict the EMG from the motion of the vertex i alone. We clip those values to a specific range $[R_{\min}, R_{\max}]$ and renormalize to $[0,1]$ in order to further weaken poorly correlated vertices (cf. Figure 5b). In all our experiments, we use $R_{\min} = 0.7$, $R_{\max} = 0.9$. The pairwise potentials (for the smoothness term in Graph Cuts) are set to a smoothing value $s = 0.6$. To improve the mask, the unary potentials for the sink and source node were weighted with a pre-factor P. Empirically we found that values $P_{sink} = 0.6$, $P_{source} = 9.0$ worked best.

The resulting mask corresponding to *Peroneus longus* on *subject 1* is shown in Figure 5d. The final mask might still contain small isolated areas on the mesh that can be easily filtered out by removing all but the largest connected area from the mask (Figure 5e). The automatically generated mask confines the muscle area very well. As we show in our experiments, the mask generalizes well to other people and is consistent across different body shapes (Figure 5f).

4.3. Principal Component Regression

The muscle mask is now used to select the vertices from $\mathbf{X}$ for supervised principal component analysis. Essentially we just run PCA on the vertices in the muscle area to obtain K principal components. These principal components correspond to the main modes of displacement in this area. We can now learn a simple linear model that maps from the PCA projection space to the EMG signal, $g : \mathbb{R}^K \to \mathbb{R}$. Notice that we could have also learned the mapping directly from the masked displacements to the EMG, but our experiments show that this leads to severe overfitting when applying the learnt model to another person. The PCA prevents this, by summarizing the collective motion in the muscle area.

5. Results

To evaluate our method, we perform a quantitative evaluation. As described in Section 3.4, we captured 4 subjects in one-leg stance. We first test if our model can estimate the EMG from 3D surface deformation on a single person in Section 5.1. We also show that the model generalizes to different persons (Section 5.2). Furthermore, in Section 5.3 the performance of different model components is compared. Ultimately, Section 5.4 shows the interpretability of our model by visualizing deformation muscle deformation.

5.1. Accuracy on Single Subject

We trained the model on two repetitions of the one-leg stance of one person and then measured the model performance on one left-out repetition. This simulates how the model generalizes to new motion of the same person. The correlation coefficient between the muscle activity predicted by the model and the real EMG is shown in Table 2. The muscular activity of *Peroneus longus* and *Tibialis anterior* can be predicted very well, because both muscles are typically active during balance tasks and their volume changes are clearly visible on the skin. Figure 6 shows that the model-estimated fits the real EMG signal very closely. The absolute estimation error is 0.009 (EMG values run in values from 0.0 to 0.2). Figure 6 also shows the 3D deformation at different points in time, thereby making it possible to see where the skin deforms. For *Peroneus longus*, deformation show up directly on the muscle and a bit on the tendon. In contrast, *Tibilias anterior* activation visually appears mostly at the tendon. The results of *Soleus* and *Gastrocnemius* are worse, presumably because these muscles are typically not very active during balance exercises.

5.2. Cross Subject Evaluation

To test how the model generalizes to new body shapes, we performed a cross subject evaluation: The model is trained on one person and then evaluated on the remaining persons. The high correlation coefficients in Figure 8 hint at excellent generalizability of our model even in face of very different physical constitutions and body shapes - especially for the muscles *Peroneus longus* and *Tibialis anterior*. Admittedly, the accuracy for subject 4 of the muscle *Peroneus longus* is suboptimal in all cases (Figure 8a). This may be related to a different muscle strategy or anomaly in the muscle of the subject. As visible in Figure 7, the trend and shape of both signals matches remarkably well. However, the model fails at estimating the correct maximal amplitude of the EMG signal when trained and tested on different subjects, cf. Figure 7. Here the absolute average estimation error is 0.03. In other words, the model estimates the EMG only up to a subject-specific factor. This happens mainly due to different constitutions of the subjects as well as due to slight differences in attachment points of the EMG electrodes.

Subject	Peron. long.	Tibial. ant.	Soleus	Gastrocnemius
#1	0.83	0.90	0.60	0.30
#2	0.88	0.89	0.78	0.74
#3	0.86	0.88	0.59	0.74
#4	0.63	0.90	0.65	0.58

Table 2: Accuracy on single subject displayed as correlation coefficients between the estimated and real EMG signal. The three results per muscle and subject were averaged for clarity.

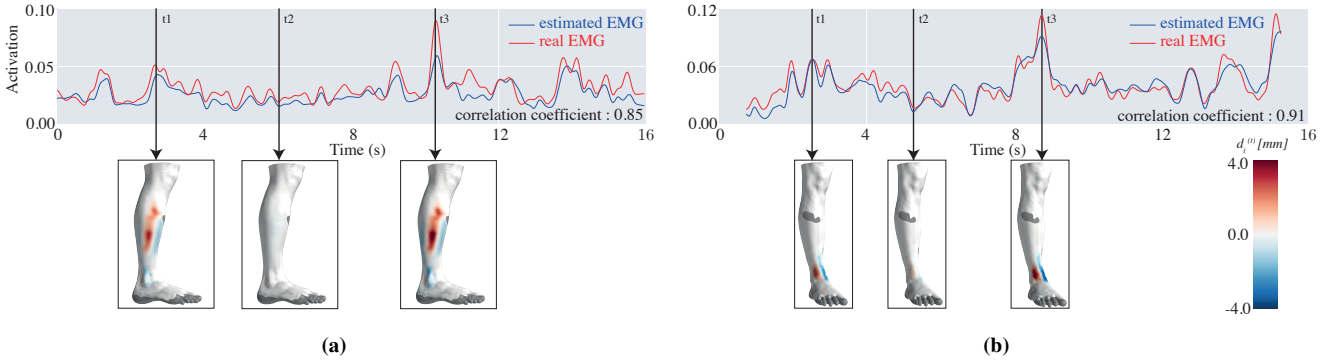

Figure 6: Result of EMG estimation for (a) *Peroneus longus* on *subject 1* and (b) *Tibialis anterior* on *subject 3* when testing on a single subject. For this, the estimated and real signal are assigned on the time axis. The y-axis represents the activation of the muscle. Furthermore, the strength of the deformation on the skin is color-coded in shape representations. For red colors there is a indentation and for blue colors a bulge. It can be seen that the deformation strength matches the muscle activation.

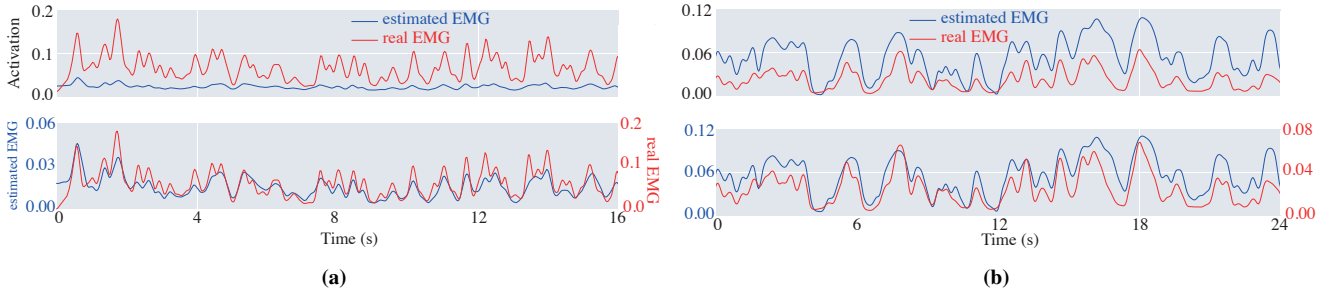

Figure 7: Time course when tested and trained on different subjects. The upper graphics show estimated and real plotted on the same axis. A large offset can be seen, which can be explained by the different value ranges of the EMG signals on different subjects. When plotted on two scaled axes, it becomes apparent that the course also agrees well. (a) *Peroneus longus*, trained on *subject 1* and tested on *subject 2* (b) *Tibialis anterior*, trained on *subject 4* and tested on *subject 1*.

	MASK	NO MASK
DIRECT	0.35	0.16
PCA	0.63	0.51

Table 3: Comparison of Model Performance: Average correlation coefficient between estimated and measured EMG (*peroneus longus* and *Tibialis anterior*, cross correlation accross all subjects) after disabling the masking (NO MASK) and/or the PCA (DIRECT) in our model. Our model with masking and PCA clearly performs best.

5.3. Comparison of Model Components

To demonstrate the importance of both muscle masking and PCA within our model, we performed an ablation study by removing those components and checking how that affects model accuracy. Instead of using the mask, we learn on the whole leg ("NO MASK"). Instead of running a PCA, we regress muscle activity directly from the displacements of all the vertices ("DIRECT"). We can see in Table 3 that both masking and especially PCA significantly improve accuracy of the model. Training the model from vertex displacements directly ("DIRECT") results in severe overfitting, as also demonstrated in Figure 9.

5.4. Visualization of Exaggerated Muscle Deformation

Another useful application is the visualization of deformation of specific muscles. Such muscle deformation are usually not clearly visible, because the deformation takes place in the range of millimeters. With our approach we are able to exaggerate muscle deformation: Instead of learning a model that maps from the PCA projection to the EMG, we learn K models (each for one principal component), that maps backwards the EMG signal to the PCA projection space, $g : \mathbb{R} \rightarrow \mathbb{R}^K$. The predicted PCA space from the EMG Signal is now weighted with a prefactor to exaggerate the shape deformation. After invers transformating the PCA space in the vertex space, the exaggerated muscle deformation can be rendered as in Figure 10. This technique is similar to that used by [GNW17], but it isolates different muscles automatically. Such a feature could be used for realistic representation of muscle deformation in character animation, but also for educational and even medical purposes to study spatial arrangement and behavior of the muscle.

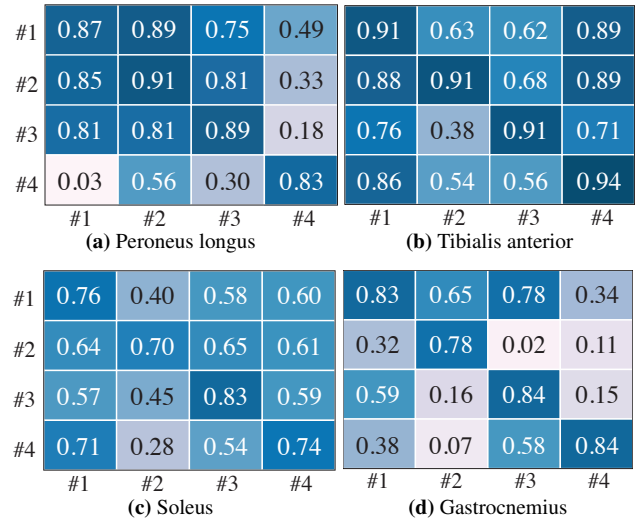

Figure 8: Accuracy on cross subject evaluation. Here, the correlation coefficients between the estimated and real EMG signal is represented. The model is trained on one subject (y-axis) and tested on another (x-axis). The results on the main diagonal are better since the model was learned and tested on the same subject.

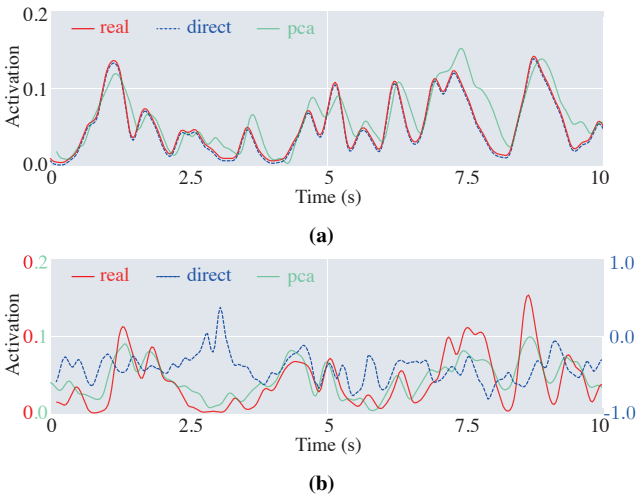

Figure 9: Comparison of PCA and DIRECT Regression. (a) Model was trained on the same trail as tested. The direct regression of the vertex displacements overfits very strongly, the signal can be almost perfectly reconstructed. In contrast, the PCA based variant overfits much less. (b) Comparison between DIRECT and PCA regression when training and testing was done on different trials. It can be seen, that PCA Regression can estimate the signal much better as DIRECT variant.

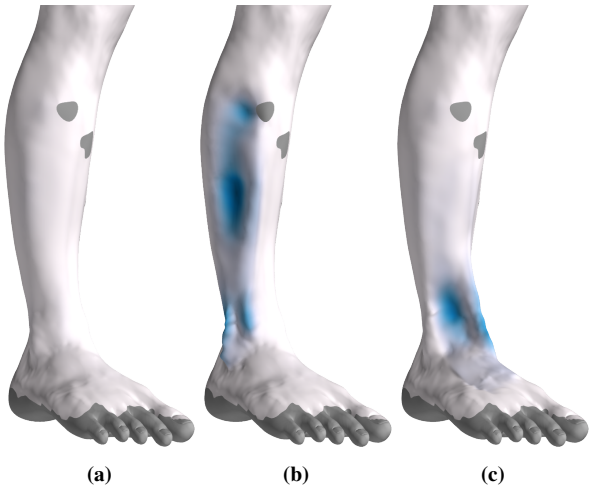

Figure 10: Muscle deformation with exaggeration by the factor of six (a) rest position (b) Peroneus longus (c) Tibialis anterior

6. Discussion

In this paper, we tackled the novel task of estimating muscle activity from high-resolution 3D recordings of the skin surface. Our method based on Supervised Principal Component Regression works reliably on certain muscles of the lower limb during the one-leg stance, even across different subjects. Nevertheless, there are some limitations that need to be fixed before our method can be tested in clinical settings.

Our pose normalization procedure fails for large motion (running, walking, jumping, etc.): linear blend skinning is (known to be) bad at modelling skin deformation during knee bends and therefore, not all pose-related deformation can be successfully subtracted. This could be fixed by adapting an existing data-based models such as [LMR*15] or by building anatomical models similar to [BB14, ZHK15]. Such models could better predict pose-related deformation and thus should be able to successfully separate the subtle muscle deformation for large motion.

Our model assumes a linear relationship between skin deformation and EMG, which is known to be correct up to about 30% for skeletal muscles [HPHG03]. Other studies suggest a nonlinear relationship and hysteresis effect [MP00] between muscle expansion and muscle activation. Here, nonlinear models and more data could yield further insights and improvements. Additionally, we observed a latency between the EMG and the 3D data. In the present work we fixed this by offsetting the EMG signal by 100 milliseconds (this lag was consistent for all subjects). In the future, we plan to carefully inspect if this is an issue in our synchronization procedure or if we are indeed observing a biological phenomenon that causes visible muscle volume changes to lag behind neurological activation. Further insights in this direction may be gained by comparing our 3D measurements to data obtained by detailed muscle structure models [Roe12], but that would require careful subject-specific registration of such models to our 3D surface data. Our system could also enable the analysis of anomalies of certain muscle movements (Figure 8a, subject 4). More data and a comprehensive

medical anamnesis of the involved patients is required to clarify whether these observations are caused by an anomaly/impairment or a model error. Furthermore, it should be investigated to what soft tissue thickness between skin surface and muscle estimation works.

While our model is able to predict the shape of the muscle activation remarkably well, it is not able to estimate the true maximal amplitude of the EMG signal. This might be fixable with better maximum voluntary contraction (MVC) normalization. However, it might also be necessary to normalize the maximum skin deformation across subjects, which again requires data from more people.

Right now, we use a dot pattern that has to be painted onto the skin. This was done on purpose to facilitate 3D reconstruction at maximum possible precision. While the dots are applied randomly and relatively quickly, such a procedure would be completely impractical in a clinical setting. Alternatively, pattern printed tights may be used. The 3D surface of the tight is a close proxy of the true skin surface and first tests with the system of [Neu16, Section 2.2] showed that muscle deformation are well visible underneath those tights and 3D reconstruction with that system could be possible in realtime. To reduce hardware costs, the number and resolution of the cameras could be gradually reduced to find out what hardware is needed to reliably estimate muscle activity.

Finally, it is worth pointing out that our system is only a proof-of-concept right now. To assess its practicability for medical/clinical applications, a large-scale medical study would be needed, with impaired and healthy subjects including different control groups.

7. Conclusion

In summary, our novel multi-sensor system records 3D surface geometry of the skin in high spatio-temporal resolution along with EMG data for the first time. With data collected from this system we showed that there is strong correlation between visible skin bulges and electrical muscle activation. Our model is able to estimate muscle activity from subtle skin deformation in one-leg stance. In the future, we would like to substantially improve the pose normalization step. We further need to extend the method in order to analyse more muscles and apply it to more complex motions as well as to a broader range of healthy and impaired subjects. 3D skin deformation as offered by our system are an interesting new modality that promises precise insights into the temporal and spatial strategies of muscle control and may lead to improved biomechanical assessment and therapy planning.

References

[ABF15] ABRAHAM L., BROMBERG F., FORRADELLAS R.: Arm muscular effort estimation from images using computer vision and machine learning. *Lecture Notes in Computer Science (including subseries Lecture Notes in Artificial Intelligence and Lecture Notes in Bioinformatics) 9456* (2015), 125–137. 2

[ASK*05] ANGUELOV D., SRINIVASAN P., KOLLER D., THRUN S., RODGERS J., DAVIS J.: SCAPE: Shape Completion and Animation of People. In *SIGGRAPH '05 ACM SIGGRAPH 2005 Papers* (2005), pp. 408–416. 2, 3

[BB14] BEELER T., BRADLEY D.: Rigid stabilization of facial expressions. *ACM Transactions on Graphics 33*, 4 (2014), 1–9. 2, 3, 8

[BHPT06] BAIR E., HASTIE T., PAUL D., TIBSHIRANI R.: Prediction by supervised principal components. *Journal of the American Statistical Association 101*, 473 (2006), 119–137. 1, 5, 6

[BRPMB17] BOGO F., ROMERO J., PONS-MOLL G., BLACK M. J.: Dynamic FAUST: Registering Human Bodies in Motion | Perceiving Systems - Max Planck Institute for Intelligent Systems. In *CVPR2017* (2017), pp. 1–10. 2

[CCS*15] COLLET A., CHUANG M., SWEENEY P., GILLETT D., EVSEEV D., CALABRESE D., HOPPE H., KIRK A., SULLIVAN S.: High-quality streamable free-viewpoint video. *ACM Transactions on Graphics 34*, 4 (2015), 69:1–69:13. 2

[CCWA13] COHEN J., COHEN P., WEST S. G., AIKEN L. S.: *Applied Multiple Regression/Correlation Analysis for the Behavioral Sciences*. Taylor & Francis, 2013. 6

[DAA*07] DELP S. L., ANDERSON F. C., ARNOLD A. S., LOAN P., HABIB A., JOHN C. T., GUENDELMAN E., THELEN D. G.: OpenSim: Open source to create and analyze dynamic simulations of movement. *IEEE transactions on bio-medical engineering 54*, 11 (2007), 1940–1950. 2

[De 97] DE LUCA C. J.: The use of surface electromyography in biomechanics. In *Journal of Applied Biomechanics* (1997), vol. 13, pp. 135–163. 2

[DTF*15] DOU M., TAYLOR J., FUCHS H., FITZGIBBON A., IZADI S.: 3D scanning deformable objects with a single RGBD sensor. In *Proceedings of the IEEE Computer Society Conference on Computer Vision and Pattern Recognition* (2015), vol. 07-12-June, pp. 493–501. 2

[EFS56] ELIAS P., FEINSTEIN A., SHANNON C.: A note on the maximum flow through a network. *IEEE Transactions on Information Theory 2*, 4 (1956), 117–119. 6

[FMV00] FRZOVIC D., MORRIS M. E., VOWELS L.: Clinical tests of standing balance: Performance of persons with multiple sclerosis. *Archives of Physical Medicine and Rehabilitation 81*, 2 (2000), 215–221. 1

[GF08] GOLOVINSKIY A., FUNKHOUSER T.: Randomized cuts for 3D mesh analysis. *ACM Transactions on Graphics 27*, 5 (2008), 1. 6

[GNW17] GASSEL S., NEUMANN T., WACKER M.: Combining biomechanical and data-driven body surface models. *ACM SIGGRAPH 2017 Posters on - SIGGRAPH '17* (2017), 1–2. 2, 7

[HPHG03] HODGES P. W., PENGEL L. H. M., HERBERT R. D., GANDEVIA S. C.: Measurement of muscle contraction with ultrasound imaging. *Muscle and Nerve 27*, 6 (2003), 682–692. 2, 8

[HRW*00] HURVITZ E. A., RICHARDSON J. K., WERNER R. A., RUHL A. M., DIXON M. R.: Unipedal stance testing as an indicator of fall risk among older outpatients. *Archives of Physical Medicine and Rehabilitation 81*, 5 (2000), 587–591. 1

[IZN*16] INNMANN M., ZOLLHÖFER M., NIESSNER M., THEOBALT C., STAMMINGER M.: Volumedeform: Real-time volumetric non-rigid reconstruction. In *Lecture Notes in Computer Science (including subseries Lecture Notes in Artificial Intelligence and Lecture Notes in Bioinformatics)* (2016), vol. 9912 LNCS, pp. 362–379. 2

[KSO10] KAVAN L., SLOAN P.-P., O'SULLIVAN C.: Fast and Efficient Skinning of Animated Meshes. *Computer Graphics Forum 29*, 2 (2010), 327–336. 3, 4

[LCF00] LEWIS J. P., CORDNER M., FONG N.: Pose space deformation. In *Proceedings of the 27th annual conference on Computer graphics and interactive techniques - SIGGRAPH '00* (2000), pp. 165–172. 3

[Lee11] LEE D.: Modeling and Simulation of Skeletal Muscle for Computer Graphics: A Survey. *Foundations and Trends® in Computer Graphics and Vision 7*, 4 (2011), 229–276. 2

[LMR*15] LOPER M., MAHMOOD N., ROMERO J., PONS-MOLL G., BLACK M. J.: SMPL : A Skinned Multi-Person Linear Model. *ACM Trans. Graphics (Proc. SIGGRAPH Asia) 34*, 6 (2015), 248:1—-248:16. 2, 3, 8

[LRI74] LÁHODA F., ROSS A., ISSEL W.: *EMG Primer: A Guide to Practical Electromyography and Electroneurography*. Springer-Verlag, 1974. 1

[MP00] MAGANARIS C. N., PAUL J. P.: Hysteresis measurements in intact human tendon. *Journal of Biomechanics 33*, 12 (2000), 1723–1727. 8

[Neu16] NEUMANN T.: Reconstruction, Analysis, and Editing of Dynamically Deforming 3D Surfaces. 2016. 2, 3, 9

[NVH*13] NEUMANN T., VARANASI K., HASLER N., WACKER M., MAGNOR M., THEOBALT C.: Capture and statistical modeling of arm-muscle deformations. *Computer Graphics Forum 32*, 2 PART3 (2013), 285–294. 1, 2, 3

[NVW*13] NEUMANN T., VARANASI K., WENGER S., WACKER M., MAGNOR M., THEOBALT C.: Sparse Localized Deformation Components. *Tog 32*, 6 (2013), 179:1—-179:10. 3

[PH08] PARK S. I., HODGINS J. K.: Data-driven modeling of skin and muscle deformation. *ACM Transactions on Graphics 27*, 3 (2008), 1. 2

[PS02] PRESTON D. C., SHAPIRO B. E.: Needle electromyography fundamentals, normal and abnormal patterns, 2002. 2

[Roe12] ROEHRLE, O., DAVIDSON, J. B. AND PULLAN A. J.: A physiologically based, multi-scale model of skeletal muscle structure and function. *Frontiers in physiology 3*, September (2012), 358. 8

[SA07] SORKINE O., ALEXA M.: As-Rigid-As-Possible Surface Modeling. *Proceedings of the fifth Eurographics symposium on Geometry processing* (2007), 109–116. 3

[SBHI15] SAMAD M., BOBZIEN J., HARRINGTON J., IFTEKHARUDDIN K.: Analysis of facial muscle activation in children with autism using 3D imaging. In *Proceedings - 2015 IEEE International Conference on Bioinformatics and Biomedicine, BIBM 2015* (2015). 2

[SSK*05] SCHOLZ V., STICH T., KECKEISEN M., WACKER M., MAGNOR M.: Garment motion capture using color-coded patterns. *Computer Graphics Forum 24*, 3 (2005), 439–447. 2

[SYA*16] SAGAWA R., YOSHIYASU Y., ALSPACH A., AYUSAWA K., YAMANE K., HILTON A.: Analyzing muscle activity and force with skin shape captured by non-contact visual sensor. In *Lecture Notes in Computer Science (including subseries Lecture Notes in Artificial Intelligence and Lecture Notes in Bioinformatics)* (2016), vol. 9431, pp. 488–501. 2

[TdAS*10] THEOBALT C., DE AGUIAR E., STOLL C., SEIDEL H.-P., THRUN S.: *Performance Capture from Multi-View Video*. Springer, 2010, pp. 127–150. 1, 2

[WCF07] WHITE R., CRANE K., FORSYTH D. A.: Capturing and animating occluded cloth. *ACM Transactions on Graphics 26*, 3 (2007), 34. 2

[ZHK15] ZHU L., HU X., KAVAN L.: Adaptable Anatomical Models for Realistic Bone Motion Reconstruction. In *Computer Graphics Forum* (2015), vol. 34, pp. 459–471. 3, 8

[ZHV*10] ZECH A., HÜBSCHER M., VOGT L., BANZER W., HÄNSEL F., PFEIFER K.: Balance training for neuromuscular control and performance enhancement: A systematic review. *Journal of Athletic Training 45*, 4 (2010), 392–403. 1

[ZNI*14] ZOLLHÖFER M., NIESSNER M., IZADI S., REHMANN C., ZACH C., FISHER M., WU C., FITZGIBBON A., LOOP C., THEOBALT C., STAMMINGER M.: Real-time Non-rigid Reconstruction using an RGB-D Camera. *ACM Trans. Graph. (TOG) 33*, 4 (2014). 3